Honey bee Odorant Binding Protein 14: Effects on Thermal Stability upon Odorant Binding revealed by FT-IR Spectroscopy and CD Measurements

Andreas Schwaighofer[†], Caroline Kotlowski[‡], Can Araman[§], Nam Chu[§], Rosa Mastrogiacomo[‖], Christian Becker[§], Paolo Pelosi,[‖] Wolfgang Knoll[†], Melanie Larisika[†], and Christoph Nowak[†,‡,*]

[†]Austrian Institute of Technology GmbH, AIT, Donau-City Str. 1, 1220 Vienna, Austria

[‡]Center of Electrochemical Surface Technology, CEST, Viktor-Kaplan-Straße 2, 2700 Wiener Neustadt, Austria

[§]Institut für Biologische Chemie, Universität Wien, Währinger Straße 38, 1090 Wien, Austria

[‖]Department of Agriculture, Food and Environment, University of Pisa, Via del Borghetto 80, 56124 Pisa, Italy

This is a post-peer-review, pre-copyedit version of an article published in European Biophysics Journal. The final authenticated version is available online at DOI: 10.1007/s00249-013-0939-4.

Abstract In the present work, we study the effect of odorant binding on the thermal stability of honey bee (*Apis mellifera* L.) odorant binding protein 14. Thermal denaturation of the protein in the absence and presence of different odorant molecules was monitored by Fourier transform infrared spectroscopy (FT-IR) and circular dichroism (CD). FT-IR spectra show characteristic bands for intermolecular aggregation through formation of intermolecular β-sheets during the heating process. Transition temperatures in the FT-IR spectra were evaluated using moving-window 2D correlation maps and confirmed by CD measurements. The obtained results reveal an increase of the denaturation temperature of the protein when bound to an odorant molecule. We could also discriminate between high and low affinity odorants by determining transition temperatures, as demonstrated independently by the two applied methodologies. The increased thermal stability in the presence of ligands is attributed to a stabilizing effect of non-covalent interactions between odorant binding protein 14 and the odorant molecule.

Keywords Odorant binding protein, *Apis mellifera*, Infrared spectroscopy, circular dichroism, ligand binding, moving window 2D spectroscopy

Introduction

Odorant binding proteins (OBPs) are the object of growing interest as biosensing elements for the fabrication of odorant sensors based on the olfactory system (Park et al. 2012a; Persaud 2012; Glatz and Bailey-Hill 2011; Lee et al. 2012b). Applications are manifold and include disease diagnostics (Sankaran et al. 2011), food safety (Di Pietrantonio et al. 2013), and environmental monitoring (Misawa et al. 2010; Capone et al. 2011). Currently, so-called "electronic noses" are based on metal oxides and conducting polymers, but biomimetic sensors promise to show higher sensitivity and selectivity combined with lower detection limits and faster response time (Sankaran et al. 2012; Park et al. 2012b; Lee et al. 2012a; Jin et al. 2012). OBPs are small acidic proteins (~13-16 kDa) present in very high concentrations (10-20 mM) at the interface between olfactory receptors and external environment (Pelosi 1994; Tegoni et al. 2000; Bohbot and Vogt 2005; Pelosi et al. 2006). Their physiological role has not yet been clarified yet, but they have been associated with transfer of the odorant molecules to the receptor proteins. Odorants predominantly are lipophilic molecules and need to be carried through the aqueous olfactory mucus of vertebrates respectively the sensillar lymph of insects to the membrane-bound olfactory receptors (Sankaran et al. 2011). The number of OBP subtypes is different for each species suggesting a role in discriminating semiochemicals.

Despite a mutual name, OBPs of vertebrates and those of insects are completely different in structure. Vertebrates OBPs are folded into 8 antiparallel β-strands and a short α-helical segment, in the typical β-barrel structure of lipocalins (Bianchet et al. 1996; Tegoni et al. 1996). OBPs of insects, instead, contain six α-helical domains arranged in a very compact and stable structure. The stability of these proteins is further increased by the presence of three interlocked

disulphide bonds (Leal et al. 1999; Scaloni et al. 1999). In the honey bee (*Apis mellifera* L.), 21 genes encode proteins of the OBP family (Foret and Maleszka 2006). OBP14 which is the subject of this study has been identified in different tissues of adult bees, as well as in larvae (Iovinella et al. 2011). Using fluorescence displacement arrays, affinities of several odorants to OBP14 have been determined and geraniol has been identified as a representative of low affinity ligands and eugenol as high affinity ligand. A crystallographic study of the three-dimensional structure of this protein and its complexes with some ligands, supports the ligand-binding experiments (Iovinella et al. 2011; Spinelli et al. 2012).

Stabilizing effects of proteins upon ligand binding have been reported for a large variety of systems (Celej et al. 2005; Moreau et al. 2010; Celej et al. 2003). Weak non-covalent forces such as hydrogen bonds as well as hydrophobic and aromatic interactions have been identified to play an important role in increasing the structural stability of the protein-ligand complexes (Williams et al. 2004; Bissantz et al. 2010; Stepanenko et al. 2008; Kumar et al. 2000). Thermal denaturation measurements employing differential scanning calorimetry or isothermal denaturation are a commonly used way to study the stability of proteins (Moreau et al. 2010). However, these methods lack the ability to provide structural information of the protein during the heating process.

Fourier-transform infrared (FT-IR) spectroscopy is an established and powerful method for investigating the structure and dynamics of proteins (Barth 2007). In FT-IR spectroscopy, the amide I (1650 cm^{-1}) and amide II (1550 cm^{-1}) bands are most commonly used for secondary structure determination of proteins. Since the OH-bending band of water overlaps with the amide I band in the IR spectrum at 1640 cm^{-1}, measurements of proteins are often performed in D_2O solution. The OD-bending band is located at ~1200 cm^{-1}, thus creating a region of relatively low

absorbance between 1500 and 1800 cm^{-1}. Upon solvent exchange, the amide II band (predominantly originating from N-H vibrations) is shifted from ~1550 to ~1450 cm^{-1}, then referred to as amide II' band. Since the amide I band is mainly composed of CO vibrations, its shift is relatively small (5-10 cm^{-1}) compared to the amide II band (Fabian and Mäntele 2006). In combination with thermal denaturation experiments, FT-IR was extensively used to reveal structural changes of proteins induced by increasing temperatures (Pedone et al. 2003; Zhang et al. 1998; Arrondo et al. 2005), including thermal transitions of the β-barrel structure of vertebrae OBPs (Marabotti et al. 2008a; Marabotti et al. 2008b; Paolini et al. 1999; Scire et al. 2009). Unlike previously applied evaluation methods, we employ moving-window two-dimensional (MW2D) correlation maps to highlight the transition points in the FT-IR spectra. MW2D correlation maps are an extension to generalized 2D correlation (2D-COS) spectroscopy but here, the spectral information is sub-divided into slices along the perturbation range and the autocorrelation intensity is plotted versus the perturbation variable. Interpretation of MW2D correlations maps is more intuitive compared to the rather complex evaluation algorithms of 2D-COS spectra and it has been proven to be an excellent tool for analyzing spectral changes caused by external perturbation (Ashton and Blanch 2010; Thomas and Richardson 2000; Du et al. 2010). Further, circular dichroism (CD) is a convenient method for studying the structure of proteins in solution (Kelly et al. 2005). To the best of our knowledge, this is the first report applying FT-IR studies to insect OBPs. We investigated the changes of thermal stability upon odorant binding of low- and high-affinity ligands to OBP14. To address this question, FT-IR and CD have been adopted to study the structural changes of the protein induced by thermal denaturation, both in the presence and in absence of odorants. The denaturation temperatures in

the FT-IR spectra were visualized by MW2D correlation maps and corroborated by CD measurements.

Materials and methods

Materials

Deuterium oxide (D_2O, 99.9% D), geraniol (2,6-Dimethyl-trans-2,6-octadien-8-ol, 98%) and eugenol (4-Hydroxy-3-methoxy-1-allyl-benzol, 99%) were provided by Sigma-Aldrich (Steinheim, Germany). Dithiobis (nitriloacetic acid butylamidyl propionate) (DTNTA, ≥95.0%) was obtained from Dojindo Laboratories (Kumamoto, Japan).

Expression and purification of OBP14

The nucleotide sequence encoding OBP14 and flanked by restriction sites NdeI and BamHI, was ligated into the expression vector pET15b (Novagen, Darmstadt, Germany), which provides a His-tag at the N-terminus of the protein. Bacterial expression was performed along with established protocols (Dani et al. 2010; Iovinella et al. 2011) and purification was accomplished using conventional chromatographic techniques (Ban et al. 2003; Calvello et al. 2003). The purity of the protein was checked by SDS-PAGE.

Infrared Spectroscopy

Infrared absorption measurements were performed using a Bruker 70v FTIR spectrometer (Karlsruhe, Baden-Württemberg, Germany), equipped with a Harrick Horizon attenuated total reflection (ATR) measuring unit with a temperature-controlled liquid sample cell (400 µL),

containing a ZnSe ATR crystal (angle of incidence ϴ = 45°, 12.5 active reflections). Recombinant OBP14 from *E. coli* with a His-tag engineered on the N-terminus was expressed as described by Iovinella et al. (Iovinella et al. 2011). ATR crystals were immersed in a solution of 5 mM DTNTA and 5 mM 3,3'-dithiodipropionic acid (DTP) in dry DMSO for 20 h. After rinsing with purified water, the crystals were immersed in 40 mM $NiCl_2$ in acetate buffer (50 mM, pH 5.5) for 30 minutes, followed by thorough rinsing with purified water to remove excess $NiCl_2$. OBP14 dissolved in phosphate buffer (140 mM NaCl, 3 mM KCl, 10 mM Na_2HPO_4, 2 mM KH_2PO_4, pH 8) was adsorbed at 25 °C onto the NTA-functionalized surface at a final concentration of 20 µM. After 4-h adsorption time, the cell was rinsed with phosphate buffer. Hydrogen/deuterium (H/D) exchange was initiated by exchanging the buffer in the measurement cell by D_2O-phosphate buffer (pD=8.0, corresponding to the pH meter reading + 0.4),(Glasoe and Long 1960) followed by pumping the deuterated buffer through the sample cell for 20 h at 0.15 mL/min. For measurements in the presence of odorants, the protein was incubated in 100 µM odorant solution in D_2O-buffer for 1 h. In thermal-denaturation experiments, the temperature was raised by 5 °C steps from 25-90 °C. Spectra were obtained after a 5 min equilibration time for stabilizing the cell temperature.

During FT-IR measurements, the sample chamber was continuously purged with dry carbon dioxide-free air, and the total reflected IR beam intensity was measured using a liquid nitrogen-cooled photovoltaic mercury cadmium telluride (MCT) detector. Spectra were recorded with a spectral resolution of 4 cm^{-1} in double-sided acquisition mode, the mirror velocity was set to 80 kHz. At least 1000 scans were taken for each spectrum, which was calculated using a Blackman-Harris 3-term apodization function and a zero filling factor of 2. Spectra were analyzed using the software package OPUS 6.5 and OriginLab's Origin software.

Moving-Window 2D correlation Spectroscopy

MW2D correlation spectra were calculated using the difference spectra after baseline correction with the freely available 2Dshige software (available at http://sci-tech.ksc.kwansei.ac.jp/~ozaki/2D-shige.htm) with a window size of 2m+1=11.

Circular Dichroism

Far UV (260-195 nm) CD measurements were carried out using an Applied Photophysics Chirascan plus spectrophotometer (Leatherhead, Surrey, United Kingdom) equipped with a temperature control unit (Quantum TC125) in a 1 mm quartz cell at 1 nm resolution. Protein solutions (0.5 mg/mL; 41.8 μM) were prepared in phosphate buffer, pH 8. For static measurements, ten spectra with the acquisition time of 0.5 s were taken at room temperature and the results were averaged. For measurement of OBP14 in the presence of odorants, the protein was incubated in 200 μM odorant solution for 1 h. In temperature-controlled experiments, spectra were taken in the range of 20-85 °C (ΔT=5 °C) with an acquisition time of 0.2 s after an equilibration time of 30 s at each temperature step. Thermal stability measurements were repeated four times.

Results and discussion

Infrared spectroscopy

OBP14 engineered with a His-tag at its N-terminus was immobilized on the NTA-linker functionalized on the ZnSe crystal (see Fig. S1 in the Supporting Information). Because of the increased noise level in the amide I region due to the high absorption of the OH-bending band of water in this area, H/D-exchange was performed to permit secondary structure determination. During exchange of the aqueous buffer with deuterated buffer solution (not shown), the amide II (~1550 cm^{-1}) band, primarily consisting of N-H bending modes, decreased and shifted to the amide II' band (~1450 cm^{-1}), that partly overlaps with the HOD vibration (1450 cm^{-1}) (Walrafen 1972). Since the N-H bending vibration only marginally contributes to the amide I band, it only exhibits a smaller shift to lower wavenumbers upon H/D exchange (Wu et al. 2001; Barth 2007; Barth and Zscherp 2002). Fig. 1 shows a FT-IR spectrum in the amide I' region of the immobilized OBP14 after H/D exchange. A curve-fit with Gaussian line shapes was performed to estimate components of the secondary structure. The measured spectrum (black line) is in good agreement with the sum of fitted lines (dashed red line). The band at 1648 cm^{-1} was attributed to α-helix, whose band position is slightly shifted to lower wavenumbers in D_2O buffer compared to aqueous buffer solution (Barth 2007; Arrondo et al. 1993; Pelton and McLean 2000). Bands at 1628.9 cm^{-1} and 1672.4 cm^{-1} were assigned to β-sheets and turns, respectively (Barth and Zscherp 2002). Evaluation of the band areas shows that the protein consists of 76.3 % α-helix, 18.9 % β-sheets and 4.8 % turns. This is in good agreement with X-ray diffraction studies that showed a high abundance of α-helix (Spinelli et al. 2012), in

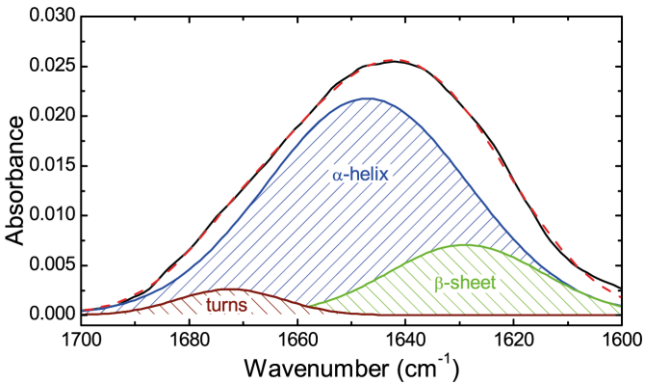

Fig. 1 FT-IR spectrum of immobilized OBP14 after H/D exchange with Gaussian curve-fits. The sum of fits (dashed red line) is in good agreement with the measured spectrum (black line)

particular when considering that curve-fitting tends to overestimate β-sheets of overly α-helical proteins at the cost of α-helix (Oberg et al. 2004; Byler and Susi 1986). For measurements in complex with geraniol and eugenol, the odorants were incubated with the protein. IR absorbance spectra of OBP14 in the presence of ligands do not show significant differences in the amide I' region compared to the bare protein spectra (see Fig. S2 in the Supporting Information). This indicates that binding of the odorant does not considerably modify the secondary structure in the protein, as reported previously for odorant binding proteins of other species (Scire et al. 2009; Paolini et al. 1999; Vincent et al. 2000; Zhou et al. 2009).

The effect of odorant binding on the thermal stability of honey bee OBP14 were determined by monitoring the amide I' band, both in the absence and presence of geraniol and eugenol during the heating process. Fig. 2a shows changes of the amide I' band while rising the temperature from 25 to 90 °C. With increasing temperature, the band shifts to higher frequencies. In spectroscopic methods, a band shift usually is the cumulative effect of the decrease of intensity at one vibration frequency combined with the increase of intensity at another vibration frequency. To study the structural changes during thermal denaturation in greater detail,

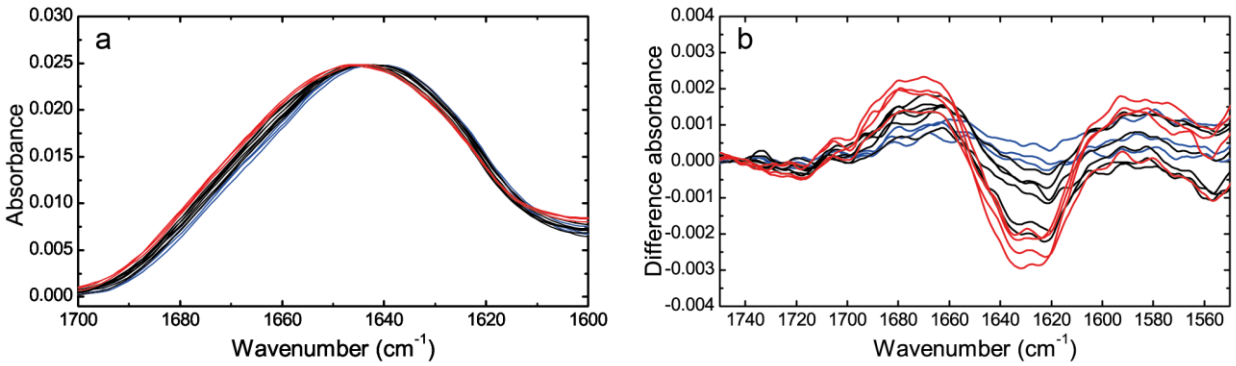

Fig. 2 (a) FT-IR spectra of OBP14 in the absence of an odorant at temperatures from 25-90 °C in the amide I' region. Spectra in blue are taken at low temperatures (30-40 °C), black spectra denote intermediate temperatures (45-70 °C) and red spectra indicate high temperatures (75-90 °C). The amide I' band shifts to higher frequencies with increasing temperature. (b) Difference spectra with the spectrum at 25 °C as a reference

difference spectra of OBP14 at various temperatures are shown in Fig. 2b. At lower temperatures up to 40 °C (blue lines), there are only minor changes in the spectra. Significant changes occur at temperatures between 40 and 70 °C (black spectra) with an increase in absorbance between 1670 and 1680 cm^{-1} and a decreasing band intensity around 1625 cm^{-1}. At high temperatures between 75 and 90 °C, only small changes take place and it seems that the structural changes upon thermal denaturation are completed. Similar behavior has been found for other α-helix-rich proteins, in particular serum albumin (Saguer et al. 2012). The negative band at ~1630 cm^{-1} is assigned to the loss of native β-sheet structure. Increasing bands in the high-frequency region can be attributed to evolving turns (~1670 cm^{-1}) and intermolecular β–sheets (~1680 cm^{-1}) due to heat induced aggregation (Saguer et al. 2012). The shift of the amide I' band to higher wavenumbers at high temperatures may also indicate an increase of disordered structures, which

have been linked to thermal denaturation (Panick et al. 1999; Ngarize et al. 2004). In several reports, intermolecular b-sheets associated to thermal aggregation are also attributed to a band at ~1620 cm^{-1} (Tatulian 2013). As depicted in Fig. 2a, this band is weakly pronounced in the present spectra. This may be due to an overlap of the decreasing portion with the native β-sheet structures, resulting in an overall negative band in the difference spectra. A further explanation for the absent band at ~1620 cm^{-1} may be a high number of turns and a lower extend of β-sheet structures. Turns and intermolecular β-sheets attributed to intermolecular aggregation are known to occur at high-temperature treatment for proteins with various native secondary structures. (Bai and Dong 2009; Pedone et al. 2003).

For visualization of the transition temperature in FT-IR spectra, MW2D correlation maps have been employed. In these maps, the FT-IR spectrum is plotted versus the perturbation coordinate, i.e. temperature. This method is particularly useful for the identification of spectral changes along the perturbation axis (Noda 2010). The temperature ranges where the largest spectral changes occur, are the regions where thermal denaturation takes place and are indicated by a peak in the correlation maps (Thomas and Richardson 2000). Fig. 3 shows the MW2D correlation maps for the thermal denaturation measurements of OBP14 in the absence or in the presence of odorants, monitored by FT-IR spectroscopy. In Fig. 3a, a sharp peak appears at 55 °C indicating that denaturation has almost completed at this temperature. Due to the nature of autocorrelation, all peaks have a positive amplitude in the MW2D correlation maps. The shape of the contour line, however, makes it possible to recognize two distinct structural elements within this peak. The high frequency peak is attributed to an increasing amount of disordered structures due to unfolding (Panick et al. 1999) and the spectral region of ~1630 cm^{-1} is attributed to a loss of native β-sheets, as discussed above. For OBP14 +

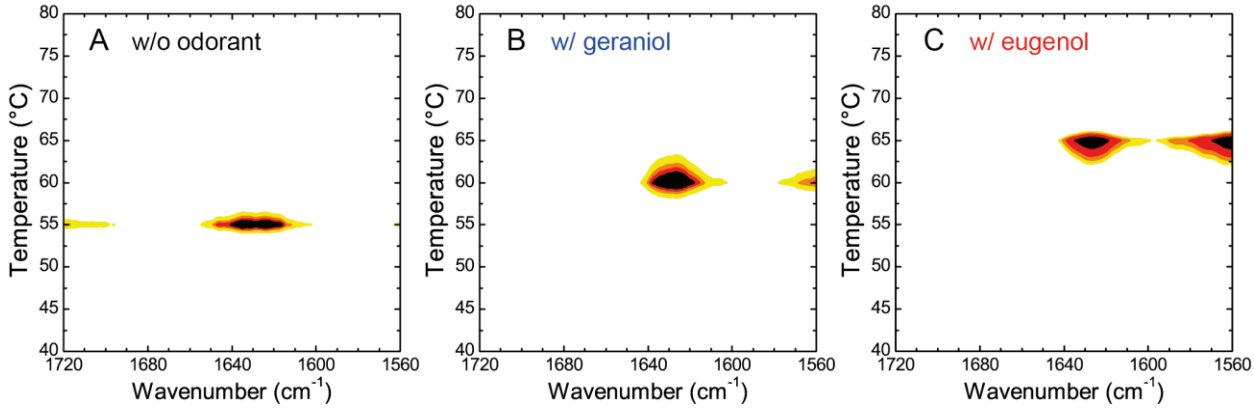

Fig. 3 MW2D correlation maps for OBP14 alone (a), or incubated with geraniol (b) and with eugenol (c)

geraniol, the peak for this structural feature is located at 60 °C (Fig. 3b), and for OBP14 + eugenol at a temperature of 65 °C (Fig. 3c). These results indicate, that the presence of odorants increases the thermal stability of the protein, and that strong ligands, such as eugenol, are more effective than weak ligands, as geraniol.

Similar thermal stabilization effects of ligands have been reported for other proteins such as porcine (Paolini et al. 1999) and bovine (Marabotti et al. 2008a) OBPs, with increase of denaturation temperature of up to 15 °C. The higher thermal stability is attributed to non-covalent forces such as hydrophobic and aromatic interactions as well as hydrogen bonds between OBP14 and the odorant molecule. Furthermore, correlation maps of OBP14 in the presence of odorants (Fig. 3b,c) display an additional peak at ~1550 cm^{-1}, that is not present in the map of OBP14 alone (Fig. 3a). Bands in this spectral region are assigned to H/D exchange. Their appearance at elevated temperatures indicates that H/D exchange has not been completed at room temperature or that prior buried structural features were exposed upon odorant binding (Paolini et al. 1999). This is in agreement with previous findings, which showed that the binding site of OBP14 undergoes geometry changes with small displacements of helices upon ligand

binding that are subject of further H/D exchange (Spinelli et al. 2012). Particularly for eugenol, it was reported that strong hydrogen bonds are involved in protein-odorant interaction (Spinelli et al. 2012), explaining the higher intensity of this peak.

Circular Dichroism

CD measurements of OBP14 were employed in the presence and absence of odorants (Fig. S3 in the Supporting Information). The spectra display two negative peaks centered at 208 nm and 222 nm, which is a clear indication of high α-helical content (Yang et al. 2011; Briand et al. 2002; Kelly and Price 2000). Hence, assignment of secondary structure of OBP14 by CD is in agreement with X-ray diffraction and IR spectroscopy, as discussed above. As in FT-IR measurements, there is no significant change of secondary structure in CD measurements at room temperature due to ligand binding.

Effects on thermal stability of OBP14 due to odorant binding were investigated by acquiring CD spectra while increasing the temperature between 20 and 85 °C in 5 °C steps (see Fig. S4 in the Supporting Information). Control measurements of the buffer and odorant solutions without protein are shown in Fig. S5 in the Supporting Information and do not reveal any changes with increasing temperatures. Thermal denaturation measurements were repeated four times and show excellent reproducibility. Denaturation transition curves and denaturation temperatures of repeated measurements are summarized in Fig. S6 and Table S1. Thermal denaturation of the protein was followed by evaluation of the CD signal at 222 nm which is particularly sensitive to changes of the secondary structure (Staiano et al. 2007; Kelly et al. 2005). Fig. 4 shows the ellipticity at 222 nm plotted versus temperature for OBP14 with and without odorants present. The data points were fitted with a Boltzmann function for sigmoidal lineshapes (dashed line).

The points of inflection i.e. the temperature of maximum change for OBP14 alone, with geraniol and with eugenol are 55, 60 and 65 °C, respectively. These results agree very well with the data obtained by FT-IR spectroscopy, thus providing another tool to demonstrate that thermal stability of OBP14, and likely other insect OBPs, is higher in the presence of ligands and depends on the strength of binding (Spinelli et al. 2012).

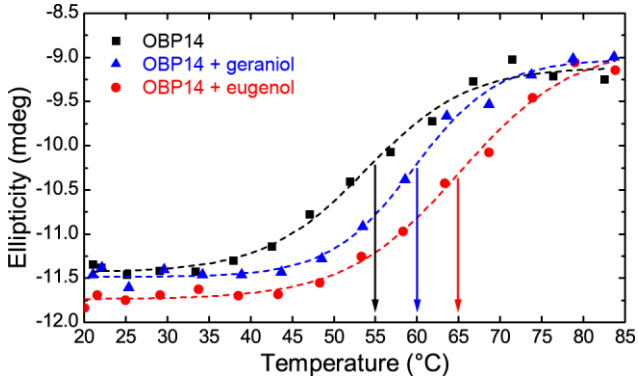

Fig. 4 Ellipticity at a wavelength of 222 nm of OBP14 in the absence and presence of odorants (data points). Dashed lines indicate a Boltzmann fit for sigmoidal lineshapes.

Conclusions

In conclusion, we have shown that the interaction of honey bee OBP14 with its ligands leads to an increase of thermal stability of the protein. This finding is corroborated by two independent analytical methods, FT-IR spectroscopy and circular dichroism. The absence of significant changes in secondary structure upon ligand binding suggests that weaker forces such as hydrogen bonds and hydrophobic interactions are involved, as previously reported for OBP14 (Spinelli et al. 2012). Low-affinity and high-affinity odorants can be discriminated by their effect

on the denaturation temperature that represents the different binding strengths and affinities for the tested odorants. Further, our measurements demonstrate the thermostability of OBP14 under ambient temperature until up to 45°C. This is of great interest with regard to possible usage of this protein in biosensor applications.

Acknowledgements

Partial support for this work was provided by the European Science Foundation (ESF), the Austrian Science Fund (FWF) (I681-N24) and the Austrian Federal Ministry for Transport, Innovation and Technology (GZ BMVIT-612.166/0001-III/I1/2010).

References

Arrondo JLR, Muga A, Castresana J, Goñi FM (1993) Quantitative studies of the structure of proteins in solution by fourier-transform infrared spectroscopy. Prog Biophys Mol Biol 59 (1):23-56.

Arrondo JLR, Pacios M, Iloro I, Goni FM (2005) Protein stability studied by 2D-infrared spectroscopy. Biophys J 88 (1):561a-562a.

Ashton L, Blanch EW (2010) pH-induced conformational transitions in alpha-lactalbumin investigated with two-dimensional Raman correlation variance plots and moving windows. J Mol Struct 974 (1-3):132-138.

Bai S, Dong A (2009) Effects of immobilization onto aluminum hydroxide particles on the thermally induced conformational behavior of three model proteins. Int J Biol Macromol 45 (1):80-85.

Ban L, Scaloni A, Brandazza A, Angeli S, Zhang L, Yan Y, Pelosi P (2003) Chemosensory proteins of Locusta migratoria. Insect Mol Biol 12 (2):125-134.

Barth A (2007) Infrared spectroscopy of proteins. Biochim Biophys Acta, Bioenerg 1767 (9):1073-1101.

Barth A, Zscherp C (2002) What vibrations tell about proteins. Q Rev Biophys 35 (04):369-430.

Bianchet MA, Bains G, Pelosi P, Pevsner J, Snyder SH, Monaco HL, Amzel LM (1996) The three-dimensional structure of bovine odorant binding protein and its mechanism of odor recognition. Nat Struct Biol 3 (11):934-939.

Bissantz C, Kuhn B, Stahl M (2010) A Medicinal Chemist's Guide to Molecular Interactions. J Med Chem 53 (14):5061-5084.

Bohbot J, Vogt RG (2005) Antennal expressed genes of the yellow fever mosquito (Aedes aegypti L.); characterization of odorant-binding protein 10 and takeout. Insect Biochem Mol Biol 35 (9):961-979.

Briand L, Swasdipan N, Nespoulous C, Bézirard V, Blon F, Huet J-C, Ebert P, Pernollet J-C (2002) Characterization of a chemosensory protein (ASP3c) from honeybee (Apis melliferaL.) as a brood pheromone carrier. Eur J Biochem 269 (18):4586-4596.

Byler DM, Susi H (1986) Examination of the secondary structure of proteins by deconvolved FTIR spectra. Biopolymers 25 (3):469-487.

Calvello M, Guerra N, Brandazza A, D'Ambrosio C, Scaloni A, Dani FR, Turillazzi S, Pelosi P (2003) Soluble proteins of chemical communication in the social wasp Polistes dominulus. Cell Mol Life Sci 60 (9):1933-1943.

Capone S, Pascali C, Francioso L, Siciliano P, Persaud KC, Pisanelli AM (2011) Odorant Binding Proteins as Sensing Layers for Novel Gas Biosensors: An Impedance Spectroscopy Characterization. In: Neri G, Donato N, d'Amico A, Di Natale C (eds)

Sensors and Microsystems, vol 91. Lecture Notes in Electrical Engineering. Springer Netherlands, pp 317-324.

Celej MS, Dassie SA, Freire E, Bianconi ML, Fidelio GD (2005) Ligand-induced thermostability in proteins: thermodynamic analysis of ANS-albumin interaction. Biochim Biophys Acta 1750 (2):122-133.

Celej MS, Montich GG, Fidelio GD (2003) Protein stability induced by ligand binding correlates with changes in protein flexibility. Protein Sci 12 (7):1496-1506.

Dani FR, Iovinella I, Felicioli A, Niccolini A, Calvello MA, Carucci MG, Qiao HL, Pieraccini G, Turillazzi S, Moneti G, Pelosi P (2010) Mapping the Expression of Soluble Olfactory Proteins in the Honeybee. J Proteome Res 9 (4):1822-1833.

Di Pietrantonio F, Cannata D, Benetti M, Verona E, Varriale A, Staiano M, D'Auria S (2013) Detection of odorant molecules via surface acoustic wave biosensor array based on odorant-binding proteins. Biosens Bioelectron 41:328-334.

Du HY, Zhou T, Zhang JH, Liu XY (2010) Moving-window two-dimensional correlation infrared spectroscopy study on structural variations of partially hydrolyzed poly(vinyl alcohol). Anal Bioanal Chem 397 (7):3127-3132.

Fabian H, Mäntele W (2006) Infrared Spectroscopy of Proteins. In: Handbook of Vibrational Spectroscopy. John Wiley & Sons, Ltd.

Foret S, Maleszka R (2006) Function and evolution of a gene family encoding odorant binding-like proteins in a social insect, the honey bee (Apis mellifera). Genome Res 16 (11):1404-1413.

Glasoe PK, Long FA (1960) Use of glass electrodes to measure acidities in deuterium oxide. J Phys Chem 64 (1):188-190.

Glatz R, Bailey-Hill K (2011) Mimicking nature's noses: from receptor deorphaning to olfactory biosensing. Prog Neurobiol 93 (2):270-296.

Iovinella I, Dani FR, Niccolini A, Sagona S, Michelucci E, Gazzano A, Turillazzi S, Felicioli A, Pelosi P (2011) Differential expression of odorant-binding proteins in the mandibular glands of the honey bee according to caste and age. J Proteome Res 10 (8):3439-3449.

Jin HJ, Lee SH, Kim TH, Park J, Song HS, Park TH, Hong S (2012) Nanovesicle-based bioelectronic nose platform mimicking human olfactory signal transduction. Biosens Bioelectron 35 (1):335-341.

Kelly SM, Jess TJ, Price NC (2005) How to study proteins by circular dichroism. Biochim Biophys Acta, Proteins Proteomics 1751 (2):119-139.

Kelly SM, Price NC (2000) The Use of Circular Dichroism in the Investigation of Protein Structure and Function. Curr Protein Pept Sci 1 (4):349-384.

Kumar S, Tsai C-J, Nussinov R (2000) Factors enhancing protein thermostability. Protein Eng 13 (3):179-191.

Leal WS, Nikonova L, Peng GH (1999) Disulfide structure of the pheromone binding protein from the silkworm moth, Bombyx mori. FEBS Lett 464 (1-2):85-90.

Lee SH, Jin HJ, Song HS, Hong S, Park TH (2012a) Bioelectronic nose with high sensitivity and selectivity using chemically functionalized carbon nanotube combined with human olfactory receptor. J Biotechnol 157 (4):467-472.

Lee SH, Kwon OS, Song HS, Park SJ, Sung JH, Jang J, Park TH (2012b) Mimicking the human smell sensing mechanism with an artificial nose platform. Biomaterials 33 (6):1722-1729.

Marabotti A, Lefevre T, Staiano M, Crescenzo R, Varriale A, Rossi M, Pezolet M, D'Auria S (2008a) Mutant bovine odorant-binding protein: Temperature affects the protein stability and dynamics as revealed by infrared spectroscopy and molecular dynamics simulations. Proteins: Struct, Funct, Genet 72 (2):769-778.

Marabotti A, Scire A, Staiano M, Crescenzo R, Aurilla V, Tanfani F, D'Auria S (2008b) Wild-Type and Mutant Bovine Odorant-Binding Proteins To Probe the Role of the Quaternary Structure Organization in the Protein Thermal Stability. J Proteome Res 7 (12):5221-5229.

Misawa N, Mitsuno H, Kanzaki R, Takeuchi S (2010) Highly sensitive and selective odorant sensor using living cells expressing insect olfactory receptors. Proc Natl Acad Sci 107 (35):15340-15344.

Moreau MJ, Morin I, Schaeffer PM (2010) Quantitative determination of protein stability and ligand binding using a green fluorescent protein reporter system. Mol Biosyst 6 (7):1285-1292.

Ngarize S, Herman H, Adams A, Howell N (2004) Comparison of Changes in the Secondary Structure of Unheated, Heated, and High-Pressure-Treated β-Lactoglobulin and Ovalbumin Proteins Using Fourier Transform Raman Spectroscopy and Self-Deconvolution. Journal of Agricultural and Food Chemistry 52 (21):6470-6477.

Noda I (2010) Two-dimensional correlation spectroscopy - Biannual survey 2007-2009. J Mol Struct 974 (1-3):3-24.

Oberg KA, Ruysschaert JM, Goormaghtigh E (2004) The optimization of protein secondary structure determination with infrared and circular dichroism spectra. Eur J Biochem 271 (14):2937-2948.

Panick G, Malessa R, Winter R (1999) Differences between the Pressure- and Temperature-Induced Denaturation and Aggregation of β-Lactoglobulin A, B, and AB Monitored by FT-IR Spectroscopy and Small-Angle X-ray Scattering. Biochemistry 38 (20):6512-6519.

Paolini S, Tanfani F, Fini C, Bertoli E, Paolo P (1999) Porcine odorant-binding protein: structural stability and ligand affinities measured by Fourier-transform infrared spectroscopy and fluorescence spectroscopy. Biochim Biophys Acta, Protein Struct Mol Enzymol 1431 (1):179-188.

Park J, Lim JH, Jin HJ, Namgung S, Lee SH, Park TH, Hong S (2012a) A bioelectronic sensor based on canine olfactory nanovesicle-carbon nanotube hybrid structures for the fast assessment of food quality. Analyst 137 (14):3249-3254.

Park SJ, Kwon OS, Lee SH, Song HS, Park TH, Jang J (2012b) Ultrasensitive flexible graphene based field-effect transistor (FET)-type bioelectronic nose. Nano Lett 12 (10):5082-5090.

Pedone E, Bartolucci S, Rossi M, Pierfederici FM, Scire A, Cacciamani T, Tanfani F (2003) Structural and thermal stability analysis of Escherichia coli and Alicyclobacillus acidocaldarius thioredoxin revealed a molten globule-like state in thermal denaturation pathway of the proteins: an infrared spectroscopic study. Biochem J 373:875-883.

Pelosi P (1994) Odorant-Binding Proteins. Crit Rev Biochem Mol 29 (3):199-228.

Pelosi P, Zhou JJ, Ban LP, Calvello M (2006) Soluble proteins in insect chemical communication. Cell Mol Life Sci 63 (14):1658-1676.

Pelton JT, McLean LR (2000) Spectroscopic methods for analysis of protein secondary structure. Anal Biochem 277 (2):167-176.

Persaud KC (2012) Biomimetic Olfactory Sensors. IEEE Sens J 12 (11):3108-3112.

Saguer E, Alvarez P, Ismail AA (2012) Heat-induced denaturation/aggregation of porcine plasma and its fractions studied by FTIR spectroscopy. Food Hydrocolloids 27 (1):208-219.

Sankaran S, Khot LR, Panigrahi S (2012) Biology and applications of olfactory sensing system: A review. Sens Actuator B-Chem 171:1-17.

Sankaran S, Panigrahi S, Mallik S (2011) Odorant binding protein based biomimetic sensors for detection of alcohols associated with Salmonella contamination in packaged beef. Biosens Bioelectron 26 (7):3103-3109.

Scaloni A, Monti M, Angeli S, Pelosi P (1999) Structural analysis and disulfide-bridge pairing of two odorant-binding proteins from Bombyx mori. Biochem Biophys Res Commun 266 (2):386-391.

Scire A, Marabotti A, Staiano M, Briand L, Varriale A, Bertoli E, Tanfani F, DAuria S (2009) Structure and Stability of a Rat Odorant-Binding Protein: Another Brick in the Wall. J Proteome Res 8 (8):4005-4013.

Spinelli S, Lagarde A, Iovinella I, Legrand P, Tegoni M, Pelosi P, Cambillau C (2012) Crystal structure of Apis mellifera OBP14, a C-minus odorant-binding protein, and its complexes with odorant molecules. Insect Biochem Mol Biol 42 (1):41-50.

Staiano M, D'Auria S, Varriale A, Rossi M, Marabotti A, Fini C, Stepanenko OV, Kuznetsova IM, Turoverov KK (2007) Stability and dynamics of the porcine odorant-binding protein. Biochemistry 46 (39):11120-11127.

Stepanenko OV, Marabotti A, Kuznetsova IM, Turoverov KK, Fini C, Varriale A, Staiano M, Rossi M, D'Auria S (2008) Hydrophobic interactions and ionic networks play an

important role in thermal stability and denaturation mechanism of the porcine odorant-binding protein. Proteins: Struct, Funct, Genet 71 (1):35-44.

Tatulian S (2013) Structural Characterization of Membrane Proteins and Peptides by FTIR and ATR-FTIR Spectroscopy. In: Kleinschmidt JH (ed) Lipid-Protein Interactions, vol 974. Methods in Molecular Biology. Humana Press, pp 177-218.

Tegoni M, Pelosi P, Vincent F, Spinelli S, Campanacci V, Grolli S, Ramoni R, Cambillau C (2000) Mammalian odorant binding proteins. Biochim Biophys Acta-Protein Struct Molec Enzymol 1482 (1-2):229-240.

Tegoni M, Ramoni R, Bignetti E, Spinelli S, Cambillau C (1996) Domain swapping creates a third putative combining site in bovine odorant binding protein dimer. Nat Struct Biol 3 (10):863-867.

Thomas M, Richardson HH (2000) Two-dimensional FT-IR correlation analysis of the phase transitions in a liquid crystal, 4'-n-octyl-4-cyanobiphenyl (8CB). Vib Spectrosc 24 (1):137-146.

Vincent F, Spinelli S, Ramoni R, Grolli S, Pelosi P, Cambillau C, Tegoni M (2000) Complexes of porcine odorant binding protein with odorant molecules belonging to different chemical classes. J Mol Biol 300 (1):127-139.

Walrafen GE (1972) Raman and infrared spectral investigations of water structure. In: Franks F (ed) Water A Comprehensive Treatise, vol 1. Plenum Press, New York, pp 151-214.

Williams DH, Stephens E, O'Brien DP, Zhou M (2004) Understanding Noncovalent Interactions: Ligand Binding Energy and Catalytic Efficiency from Ligand-Induced Reductions in Motion within Receptors and Enzymes. Angew Chem, Int Ed 43 (48):6596-6616.

Wu Y, Murayama K, Ozaki Y (2001) Two-Dimensional Infrared Spectroscopy and Principle Component Analysis Studies of the Secondary Structure and Kinetics of Hydrogen-Deuterium Exchange of Human Serum Albumin. J Phys Chem B 105 (26):6251-6259.

Yang G, Winberg G, Ren H, Zhang SG (2011) Expression, purification and functional analysis of an odorant binding protein AaegOBP22 from Aedes aegypti. Protein Expres Purif 75 (2):165-171.

Zhang HM, Ishikawa Y, Yamamoto Y, Carpentier R (1998) Secondary structure and thermal stability of the extrinsic 23 kDa protein of photosystem II studied by Fourier transform infrared spectroscopy. Febs Letters 426 (3):347-351.

Zhou J-J, Robertson G, He X, Dufour S, Hooper AM, Pickett JA, Keep NH, Field LM (2009) Characterisation of Bombyx mori Odorant-binding Proteins Reveals that a General Odorant-binding Protein Discriminates Between Sex Pheromone Components. Journal of Molecular Biology 389 (3):529-545.